Colloid Polym Sci (2014) 292:2811–2820
DOI 10.1007/s00396-014-3332-7

ORIGINAL CONTRIBUTION

# Detection of trace levels of atrazine using surface-enhanced Raman scattering and information visualization

**Rafael J. G. Rubira · Sabrina A. Camacho · Pedro H. B. Aoki · Mateus D. Maximino · Priscila Alessio · Cibely S. Martin · Osvaldo N. Oliveira Jr. · Francisco M. Fatore · Fernando V. Paulovich · Carlos J. L. Constantino**

Received: 15 May 2014 / Revised: 1 July 2014 / Accepted: 2 July 2014 / Published online: 17 July 2014


**Abstract** The detection of trace amounts of pesticides is essential for the quality control of waters, particularly with their inevitable increasing use with the growing demand for food. In this study, we report on the detection of atrazine, a highly toxic herbicide, down to $5\times10^{-12}$ M, which is sufficient to monitor the quality of drinking water even according to the most stringent international regulations. Such detection was performed with surface-enhanced Raman scattering (SERS) in atrazine incorporated into silver nanoparticles (AgNPs) colloids, with the SERS spectra being treated with Sammon's mapping, an information visualization technique. In addition to providing a fingerprint of the atrazine molecules, SERS is advantageous in comparison with impedance spectroscopy and cyclic voltammetry applied to a sensor array of units made with layer-by-layer (LbL) films containing AgNPs and AuNPs. The combined use of SERS and information visualization methods is promising for monitoring water quality with regard to other pesticides, which may even approach single molecule detection.

**Keywords** Pollutant · Atrazine · SERS · Sensor array · Information visualization

## Introduction

The growing demand for food with the increase in the world's population has sparked the need of enlarged cultivated areas and an increase in productivity in agriculture, thus generating an increasing use of pesticides. Unfortunately, some of these pesticides are not biodegradable and have limited solubility in aqueous solutions, which can then lead to contamination of the environment, especially for groundwater and drinking water. One of such pesticides is atrazine, a widely used herbicide [1], which acts as an inhibitor of photosynthesis [2, 3] and may present endocrine disruptor or carcinogenic effects depending on its concentration [4–6]. It is not easily biodegraded due to its low solubility. Thus, it is necessary to develop more sensitive and selective analytical methods to monitor residual amounts of this pesticide.

In a search in the literature, we found distinct reports describing a few analytical methods to detect atrazine. The chromatographic methods [7, 8] show great selectivity and sensitivity; however, they demand sophisticated sample preparation. Electrochemical sensors using mercury [9, 10] and solid electrodes [11–14] are the most explored for atrazine detection. However, besides the mercury, their detection limit is normally around $10^{-6}$ to $10^{-9}$ M, which means that in many cases such sensors are not useful to ensure quality control of drinking water. The low concentrations allowed in drinking water according to regulations in different countries vary from 3 μg/L ($1.39\times10^{-8}$ M or 3 ppb) in the USA, determined by the US Environmental Protection Agency (USEPA) [15], to 0.1 μg/L ($4.64\times10^{-10}$ M or 0.1 ppb) in the European Union [16].

**Electronic supplementary material** The online version of this article (doi:10.1007/s00396-014-3332-7) contains supplementary material, which is available to authorized users.

R. J. G. Rubira (✉) · S. A. Camacho · P. H. B. Aoki · M. D. Maximino · P. Alessio · C. S. Martin · C. J. L. Constantino
DFQB, Faculdade de Ciências e Tecnologia, UNESP Univ Estadual Paulista, Presidente Prudente, SP 19060-900, Brazil
e-mail: rafael.gon.fis@gmail.com

O. N. Oliveira Jr.
São Carlos Institute of Physics, University of São Paulo, CP 369, São Carlos, SP 13560-970, Brazil

F. M. Fatore · F. V. Paulovich
Institute of Mathematical Sciences and Computing, CP 668, São Carlos, SP 13560-970, Brazil

Since atrazine possesses a relatively strong Raman signal, we were motivated to try and detect it using surface-enhanced Raman scattering (SERS) [17], in which a signal enhancement between $10^3$ and $10^6$ can be achieved [18, 19], making it possible to be applied to diluted systems [20, 21]. The enhancing phenomenon is achieved by placing the target molecules close enough (touching) to metallic nanoparticles. The enhancement factors depend on the size, shape, and aggregation of nanoparticles; dielectric functions of the surrounding medium and of the metal (nanoparticle); and the frequency of the exciting radiation. Nanoparticles of noble metals are normally applied with exciting radiations (lasers) in the visible range [18, 19], as these nanoparticles can sustain localized surface plasmon resonances (LSPRs) that are able to amplify the electric field surrounding them. This, in turn, increases the induced dipole of the target molecule placed near the metallic nanoparticle, which is in the origin of the SERS phenomenon [18, 19]. For molecules placed in the interstices of nanoparticles (hot spots), the enhancement factor can reach up to $10^{10}$, with which single molecules can be detected [22–24]. SERS has been applied in sensing experiments under various experimental conditions, with isolated nanoparticles, colloids, and films, and for a variety of target molecules, including pesticides [20, 25–28].

In this study, we report on atrazine detection with SERS using Ag colloids for concentrations between $10^{-7}$ and $10^{-12}$ M. For comparison purposes, we also used impedance spectroscopy with a sensor array as in typical work of electronic tongues [29, 30] and cyclic voltammetry [31], in a methodology that has been applied to detect environmental pollutants. In such measurements, the sensing units were made of a bare electrode (Pt interdigitated for impedance and indium tin oxide (ITO) for cyclic voltammetry), and electrodes were coated with layer-by-layer (LbL) films containing gold or silver nanoparticles (AuNPs or AgNPs). The cartoon in Fig. 1a, b illustrates the approach applied to SERS, impedance, and voltammetric measurements. The data were analyzed using multidimensional projection techniques in order to demonstrate the viability of distinguishing trace amounts of atrazine, whose molecular structure is given in Fig. 1c.

## Materials and methods

### Reagents

The following reagents were acquired from Sigma-Aldrich: silver nitrate ($AgNO_3$, molar mass (MM)=169.88 g/mol), gold(III) chloride trihydrate ($HAuCl_4 \cdot 3H_2O$, MM=393.83 g/mol), sodium citrate ($C_6H_5Na_3O_7 \cdot 2H_2O$, MM=294.10 g/mol), hydroxylamine hydrochloride ($NH_2OH \cdot HCl$, MM=69.49 g/mol), sodium hydroxide (NaOH, MM=40.00 g/mol), and poly(allylamine hydrochloride) (PAH, MM=15,000 g/mol) polyelectrolyte. The atrazine pesticide ($C_8H_{14}ClN_5$, MM=215.68 g/mol), purity=98.8 %, was purchased from Fluka Analytical. All the chemicals were used without further purification. Ultrapure water with resistivity of 18.2 MΩ cm and pH 5.6, acquired from a Milli-Q system, model Simplicity, was used to prepare the solutions and LbL films.

### Au colloid synthesis by citrate reduction

The AuNPs were obtained by citrate reduction of $HAuCl_4$, following the method proposed by Lee and Meisel [32], and used as synthesized. They were prepared by dissolving 240 mg of $HAuCl_4$ in 500 mL of ultrapure water and heated up to boiling point. Then, 50 mL of an aqueous solution of sodium citrate 1 % water/volume (*w*/*v*) was added into the first solution under stirring, which was kept boiling and stirring for 1 h [32]. The final concentration of the AuNPs dispersion is ca 1.0 mM.

### Ag colloid synthesis by hydroxylamine reduction

The AgNPs obtained by hydroxylamine reduction were synthesized according to the methodology described by Leopold and Lendl [33]. The synthesis consisted in adding 4.5 mL aqueous solution of NaOH 0.1 M, at room temperature, into 5 mL of $NH_2OH \cdot HCl$ 43.3 mM solution. This solution was added to 90 mL of $AgNO_3$ at 1.2 mM under stirring. The final concentration of AgNPs dispersion is ca 1.0 mM [33].

### Impedance spectroscopy

The sensing units for impedance spectroscopy characterization were fabricated by the modification of Pt interdigitated electrodes through deposition of LbL films, which were grown following the experimental procedure reported in Aoki et al. [34]. Briefly, the electrode was immersed into distinct solutions according to the following sequence: PAH solution (3 min)→ultrapure water gently stirred to remove nonadsorbed PAH (1 min)→AgNPs or AuNPs colloidal dispersion (3 min)→ultrapure water to remove nonadsorbed nanoparticles (1 min). This four-step sequence led to the first bilayer, and multilayered LbL films were grown by repeating this sequence. The growth of PAH/AgNPs and PAH/AuNPs is depicted in Fig. SI1 in the Supporting Information.

The impedance spectroscopy measurements were carried out with a Solartron 1260A impedance analyzer. The sensor array was composed of three sensing units: a bare Pt interdigitated electrode and Pt interdigitated electrodes coated with five-bilayer LbL films of PAH/AuNPs and PAH/AgNPs. The bare Pt electrode is used to monitor any change in the electrical response caused by the thin films. This sensing array was

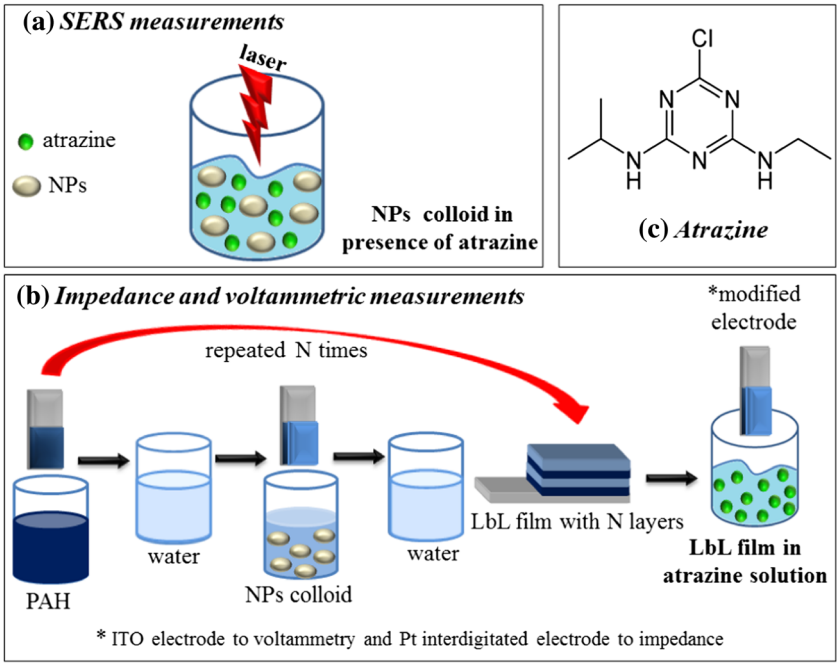


**Fig. 1** **a** Atrazine in Ag colloid for SERS measurements. **b** Immersion of LbL film of PAH/AgNPs and PAH/AuNPs into atrazine aqueous solution for impedance spectroscopy (electrode: Pt interdigitated coated by LbL film) and cyclic voltammetry (electrode: ITO coated by LbL film) measurements. *PAH*. **c** Atrazine molecular structure

applied to discriminate ultrapure water and atrazine aqueous solutions at $1.1\times10^{-10}$, $1.1\times10^{-9}$, $1.7\times10^{-8}$, $5.6\times10^{-8}$, and $1.1\times10^{-7}$ M prepared by adding aliquots of atrazine aqueous solutions from a stock solution into ultrapure water. Impedance was measured as a function of frequency from 1 up to $10^6$ Hz, with AC voltage of 50 mV. The Pt interdigitated electrodes contained 50 pairs of digits, each digit being 10 μm wide, 0.5 mm long, and 100 nm high, spaced by 10 μm from each other. The theoretical fitting of the experimental curves was carried out using the ZView software.

## Raman scattering and UV-Vis absorption spectroscopy

Micro-Raman analysis and optical microscopy were obtained using a micro-Raman Renishaw spectrograph, model inVia, equipped with a Leica microscope, whose×50 objective lens allows for collecting the spectra with ca 1 $\mu m^2$ spatial resolution. The spectrograph contains a charge-coupled device (CCD) detector, laser at 633 nm, 1,800 grooves per millimeter grating with additional edge filters. UV-Vis absorption spectra were collected using a spectrophotometer Varian, model Cary 50.

## Solutions for SERS measurements

An atrazine stock solution at $1.0\times10^{-4}$ M was diluted in Ag colloid to achieve the SERS effect. The final solution concentrations of atrazine were $5.0\times10^{-7}$, $5.0\times10^{-8}$, $5.0\times10^{-9}$, $5.0\times10^{-10}$, $5.0\times10^{-11}$, and $5.0\times10^{-12}$ M. The stock solution was prepared by dissolving 5.40 mg of atrazine in 250 mL of ultrapure water under sonication. In order to acquire SERS spectra, a small droplet of atrazine solution was placed in a holder under the microscope, and the laser focus was adjusted onto the air/water interface.

## Data analysis

Data from sensing and biosensing experiments have long been treated with statistical methods, such as principal component analysis (PCA), which is a statistical tool employed to reduce the dimensionality of the data [35]. For biosensing, in particular, other multidimensional projection techniques have been proven superior to PCA [36], especially in the cases where an optimization procedure is exploited. In these methods that are said to belong to the realms of information visualization, one attempts to project data from a multidimensional space onto a 2D or 3D plot with maximum preservation of similarity relationships. Formally, the data in the original space are represented by $X=\{x_1,x_2,..,x_n\}$, and $\delta(x_i, x_j)$ is defined as the distance between two data instances i and j. They are projected onto a 2D plot with graphical markers represented by $Y=\{y_1,y_2,..,y_n\}$, which are determined in an optimization procedure using an injective function f: $X\rightarrow Y$ that minimizes $|\delta(x_i, x_j)-d(f(x_i),f(y_j))|\approx0$, $\forall x_i, x_j\in X$ [37], where $d(y_i, y_j)$ is the distance function on the projected plane. The flexibility of this optimization approach arises from the availability of several cost (or error) functions used for placing the graphical markers on the 2D plot. Here, we used the so-called Sammon's mapping [38] and Interactive

Document Map (IDMAP) [39], whose error functions are defined, respectively, as follows:

$$S_{Sam} = \frac{1}{\sum_{i<j} \delta(x_i, x_j)} \sum \frac{\left(d(y_i, y_j) - \delta(x_i, x_j)\right)^2}{\delta(x_i, x_j)} \quad (1)$$

where $\delta$ and $d$ are the distance functions defined above and

$$S_{IDMAP} = \frac{\delta(x_i, x_j) - \delta_{\min}}{\delta_{\max} - \delta_{\min}} - \left(y_i, y_j\right) \quad (2)$$

where $\delta_{min}$ and $\delta_{max}$ are the minimum and maximum distances between the samples.

### Cyclic voltammetry

The voltammetric measurements were carried out in a voltammetric cell of three electrodes: Ag/AgCl as the reference electrode, Pt wire as the counter electrode, and ITO electrode modified with a ten bilayer LbL film of PAH/AgNPs or ten bilayer LbL film of PAH/AuNPs as working electrodes. The study of the interaction of atrazine/modified electrode was carried out by adding aliquots from $4.95\times10^{-7}$ M of atrazine standard solution containing 0.1-M KCl solution as supporting electrolyte (pH 1.88). The analyses were conducted in continuous flux of high-purity nitrogen gas. All solutions were prepared using the ultrapure water (18.2 MΩ cm).

## Results and discussion

### Sensing atrazine with SERS

SERS was applied to detect atrazine solutions down to $5\times10^{-12}$ M concentration, using Ag colloid. Figure 2 shows the SERS spectra collected for all atrazine concentrations diluted in the Ag colloid. A typical spectrum for the Ag colloid is given as reference for the identification of the atrazine vibrational bands. The several Ag colloid spectra recorded are given in the Supporting Information (Fig. SI2). There is an overlap of bands between 1,339 to 1,619 $cm^{-1}$ for atrazine and Ag colloid spectra. According to Costa et al. [40], atrazine bands in this spectral region are assigned to $CH_3$+CH+NH bending at 1,339 $cm^{-1}$, NH+CH bending+$CH_2$ wagging at 1,365 $cm^{-1}$, $CH_3$ bending at 1,453 $cm^{-1}$, and NH bending+C–N stretching at 1,619 $cm^{-1}$.

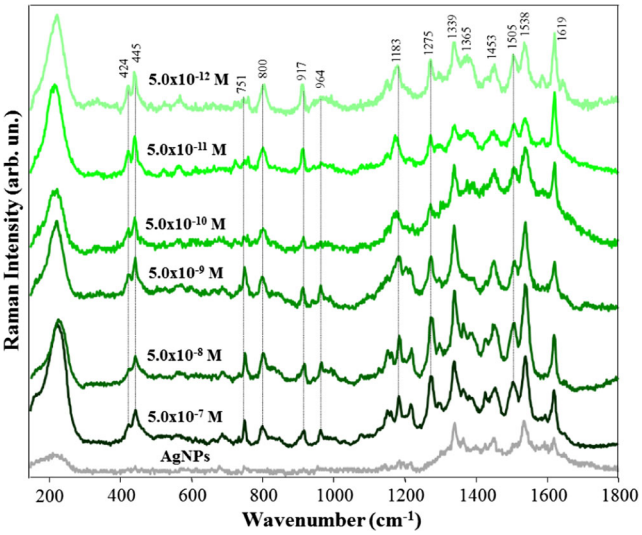


**Fig. 2** SERS spectra of atrazine solutions diluted in Ag colloid at $5.0\times10^{-7}$, $5.0\times10^{-8}$, $5.0\times10^{-9}$, $5.0\times10^{-10}$, $5.0\times10^{-11}$ and $5.0\times10^{-12}$ M concentrations. The Ag colloid spectrum is given as a reference at the bottom in order to distinguish the vibrational bands of atrazine

Vibrational bands arising only from SERS of atrazine solution are highlighted by dotted lines, with the following assignments: $CH_2$ rocking+$CH_3$ wagging at 751 $cm^{-1}$, C–C stretching+$CH_3$ wagging at 800 $cm^{-1}$, $CH_3$ twisting at 917 $cm^{-1}$, C–C stretching at 964 $cm^{-1}$, NH bending at 1,183 $cm^{-1}$, $CH_2$ twisting at 1,275 $cm^{-1}$, and NH bending at 1,505 $cm^{-1}$ [40]. The SERS spectrum of atrazine solution at $5.0\times0^{-7}$ M is compared in Fig. SI3 with the SERS spectrum of the cast film made with the same solution concentration and with the Raman spectrum of atrazine powder. The main vibrational bands in the SERS spectra for the solution and cast film and in the conventional Raman for the powder are highlighted by dotted lines. Most of SERS bands are shifted in relation to the Raman bands of the atrazine powder, which is explained by the different environments for the atrazine molecules, as discussed further later on in this paper. The average intensity of SERS was higher for the spectra collected in solution ($5.0\times10^{-7}$ M) than that in the cast film, which means that the conformation of atrazine molecules adsorbed on AgNPs plays a central role in this ultrasensitive analysis [40, 41].

According to Costa et al. [40], the isopropyl group of atrazine molecule causes a steric effect, avoiding the approximation of AgNPs in this region of the molecule. They proposed that the atrazine molecule adsorbs onto AgNPs via the N between the ethyl radical and the Cl atom. This hypothesis was confirmed by Bonora et al. [41], which observed a band at 1,610 $cm^{-1}$ assigned to the deformation of the ring due to the vibration of the C–N–H atoms positioned between the ethyl radical and Cl atom. Here, we can assume the same adsorption mechanism of the atrazine molecule onto AgNPs once the

observed bands in our SERS spectra are all related to the molecular vibrations at this position.

We have also performed a quantitative computational analysis of the SERS spectra using a multidimensional projection technique, whose details are given in Paulovich et al. [42] and Oliveira et al. [36]. The suitability of SERS to distinguish atrazine solutions demonstrated in Fig. 2 is revealed by treating the SERS spectra using the Sammon's mapping [38] technique to project the data in a 2D plot, as shown in Fig. 3. We also obtained the visualization with IDMAP, but the distinction appeared slightly superior with the Sammon's mapping. The results are clustered according to the similarity of analyzed solutions. The closer the circles, the more similar the SERS spectra are. The spectra corresponding to different atrazine concentrations are positioned apart from each other, indicating that these samples can be clearly distinguished down to $5\times10^{-12}$ M. The latter highlights the usefulness of projection techniques not only to handle the data but also to optimize the sensing performance.

The large dispersion in the data for the lowest concentration ($5\times10^{-12}$ M) could be expected on the basis of fluctuations on the SERS spectra affecting bandwidth, band shape, Raman shift, and absolute and relative intensities when approaching highly diluted solutions. Indeed, we observed such SERS spectral variation in experiments of single-molecule detection, which is associated with local changes of the molecular environment [43]. For $5\times10^{-12}$ M, the number of atrazine molecules per picoliter ($10^{-12}$ L) is estimated to be three, where the picoliter scale was chosen because this is the order of magnitude of the volume probed by the laser in single-molecule experiments [44, 45]. To our knowledge, this is the lowest concentration ever detected for atrazine solutions, approaching single-molecule levels. In fact, only a few reports regarding atrazine detection by SERS are found [40, 46]. In references Costa et al. [40] and Bonora et al. [41], the main goal was to determine how the atrazine is adsorbed onto the nanoparticle surfaces under distinct experimental conditions, and the atrazine concentrations used were $10^{-7}$ M and in the ppm range, respectively. Carrillo-Carrion et al. [46] coupled chromatography and SERS for sensing experiments, reaching a detection limit of ca 0.9 μM.

## Sensing atrazine with impedance spectroscopy

The combination of interdigitated electrodes, ultrathin films, and impedance spectroscopy is a well-established approach to detect trace levels of different analytes, including water pollutants [30, 47]. As a complementary approach, the performance of PAH/AgNPs LbL films as transducers in sensing units was checked by immersing it into aqueous solutions containing atrazine at different concentrations. Besides the five bilayers of the PAH/AgNPS LbL film, the sensor array was composed of a bare Pt interdigitated electrode and a Pt electrode coated with five bilayers of PAH/AuNPs. Figure 4a, b shows the Bode plots with capacitance versus frequency (C vs. f) curves and the Nyquist plots (Z″ vs. Z′), respectively, for all sensing units immersed into ultrapure water. As expected, even nanostructured films affect the electrical response of the Pt electrode, whose impedance curves were modeled with electrical equivalent circuits (EEC)s inspired in the work by Taylor and Macdonald [48]. The circuit in Fig. 4c corresponds to an electrode coated by an insulating film dipped in an electrolyte solution, with the film being represented by the elements CPEb and Rb in series with the electrolyte impedance. The latter contains three components: the geometric capacitance of the electrode immersed in an electrolyte (CPEg), the electrical double layer capacitance (CPEd), and the total resistance of the electrolyte represented by (1/Rd+1/Rt), where Rd is the electrical double layer resistance and Rt is the charge transfer though the interface

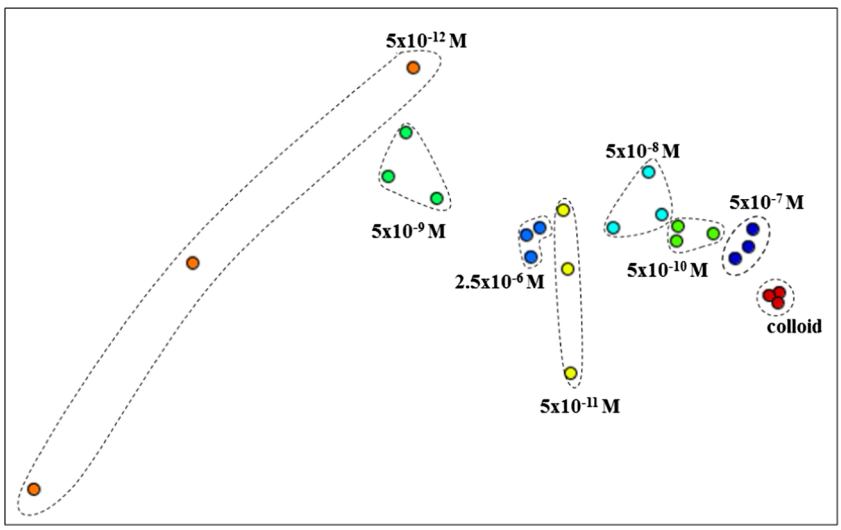


**Fig. 3** Sammon's mapping layout of the SERS spectra obtained from distinct atrazine solutions. No labels are assigned to the axes because in this type of plot what matters is the relative distance between data points, where similar samples should be placed close to each other

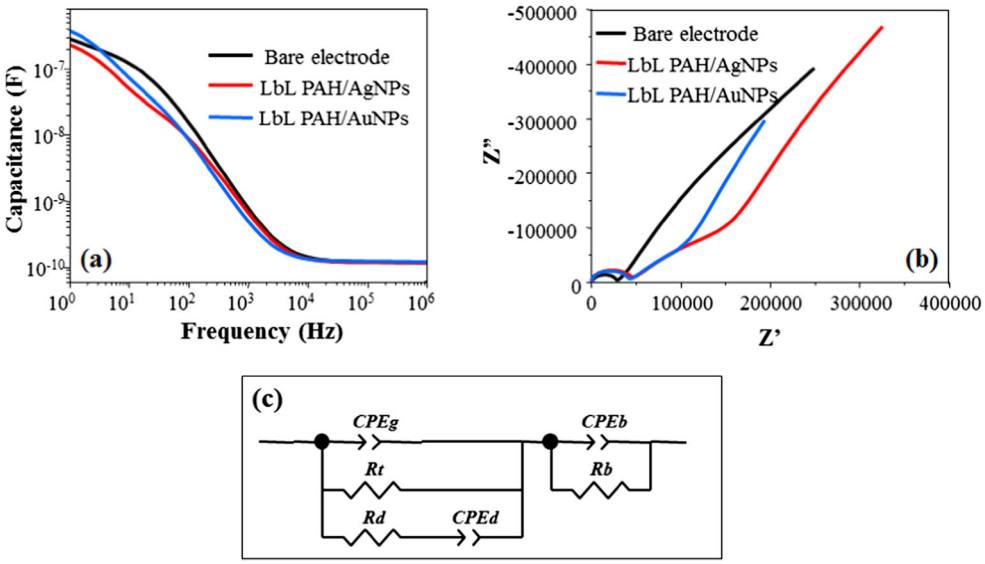


**Fig. 4** **a** Capacitance versus frequency (C vs. f) curves, **b** Nyquist plot (Z″ vs. Z′) for all sensing units immersed into ultrapure water, and **c** electrical equivalent circuit proposed by Taylor and Macdonald. *Dotted curves* are the experimental results, and *solid lines* represent the theoretical fittings in **a** and **b**. In **c** *CPEg* is the geometric capacitance of the electrode, *CPEd* is the electrical double-layer capacitance, *Rd* is the electrical double-layer resistance, *Rt* is the charge transfer resistance through the electrolyte/film interface, *CPEb* and *Rb* are the capacitance and resistance of the film coating the electrode, respectively

electrolyte/film. The electrical response is governed by different physicochemical phenomena depending on the frequency range, as follows [49]: At the low-frequency region ($10^0$–$10^2$ Hz), impedance is mainly related to the formation of an electrical double layer at the film/solution interface [49]; in the mid-frequency region ($10^2$–$10^5$ Hz), it is related to the properties of the film coating the electrode [49], and at the high-frequency region (>$10^5$ Hz), the impedance response is dominated by the geometric capacitance of the interdigitated electrodes [49] and by the dielectric constant of the solution [50].

The major changes induced by the LbL films occur at low and intermediate frequencies, as predicted by the model of Taylor and Macdonald. The parameters used for fitting are shown in Table 1, where optimized fitting was obtained upon removing the Rb element (film resistance) in the EEC, suggesting that the sensing units used here present a dominant capacitive behavior. Upon film deposition, the charge transfer resistance Rt decreased by one order of magnitude, probably owing to the presence of metallic nanoparticles, while the double-layer resistance Rd increased owing to an increased surface area for the coated electrodes, which also caused the film capacitance CPEb to decrease.

The capacitance versus frequency curves for the sensing units made with LbL films PAH/AgNPs and PAH/AuNPs are shown in Fig. 5, and the data for the bare electrode are not shown lest the plot would be overcrowded. A visual inspection does not allow one to infer whether it is possible to distinguish the samples with different atrazine concentrations, which is the reason why we resorted to statistical and computational methods for analyzing the data.

When the data for the three sensing units are combined, the projections onto a 2D plot with PCA [35] and IDMAP [39] show clear separation according to the atrazine concentration. This is illustrated in Fig. SI4 in the Supporting Information for PCA and in Fig. 6 for IDMAP, in both cases with a shift of the clusters to the right with increasing atrazine concentrations. We also used Sammon's mapping for comparison, but the results with IDMAP were superior. An interesting feature in the plot is that a measurement with ultrapure water at the end of the experiments indicated that the sensing units were affected by the measurements since the data points for "final water" did not coincide with those of the "initial water." Therefore, though it is clear that the addition of small aliquots of atrazine solution to increase the concentration leads to changes in the electrical response, thus corresponding to a high sensitivity, such changes are irreversible. As in similar work with other analytes [45, 30], irreversible adsorption on the LbL films may occur, with adsorbed molecules not being removed in the washing procedures. In Aoki et al. [45], such adsorption was confirmed with SERS experiments, but this could not be done here because the SERS signal for the LbL films was negligible. Caution should then be taken in

**Table 1** Parameters used for fitting the impedance curves of bare Pt electrode, PAH/AgNPs, and PAH/AuNPs sensing units immersed in ultrapure water

| E | CPEg | CPEg-α | Rt | Rd | CPEd | CPEd-α | CPEb | CPEb-α |
|---|---|---|---|---|---|---|---|---|
| Bare Pt | $1.23\times10^{-10}$ | 1 | $2.25\times10^{6}$ | 26143 | $4.77\times10^{-7}$ | 0.81 | $1.06\times10^{-5}$ | 0.37 |
| PAH/AgNPs | $1.65\times10^{-10}$ | 0.98 | $1.55\times10^{5}$ | 65755 | $1.32\times10^{-7}$ | 0.70 | $4.79\times10^{-7}$ | 0.79 |
| PAH/AuNPs | $1.82\times10^{-10}$ | 0.97 | $1.14\times10^{5}$ | 67947 | $2.46\times10^{-7}$ | 0.67 | $7.30\times10^{-7}$ | 0.83 |

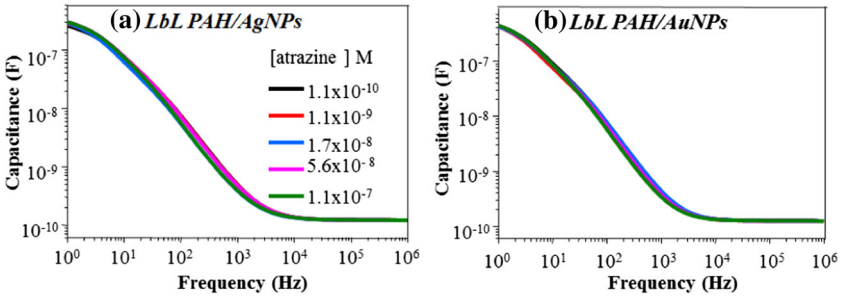


**Fig. 5** Capacitance versus frequency curves for **a** PAH/AgNPs and **b** PAH/AuNPs sensing units immersed into atrazine aqueous solution with concentrations from $1.1\times10^{-10}$ up to $1.1\times10^{-7}$ M

analytical procedures, for the results may depend on the order with which the experiments are performed. This is clearly a disadvantage of the impedance spectroscopy, compared with SERS which does not suffer from this limitation. Owing to this limitation, we have not attempted to detect even lower concentrations of atrazine to try and match the experiments for SERS.

The IDMAP technique can also be used to identify the contribution from each sensing unit for the distinction ability. The color of the circles denotes the sensing unit as indicated in the label, while the concentration is shown next to each circle in the plot. The closer the circles, the more similar the electrical responses are. The latter allows a direct visualization of the performance of each sensing unit in discriminating atrazine solutions. The bare Pt electrode is positioned apart from the other sensing units, confirming that the modification introduced by coating the Pt electrodes is significant. The results of the sensing unit composed of the PAH/AgNPs LbL film are placed separately from those of the PAH/AuNP sensing unit. There are no overlapping areas among those data. Therefore, the replacement of AgNPs for AuNPs in the LbL films gives rise to distinct data points in the plot, showing that both sensing units play a role, i. e., there is clear dependence of the electrical response on the metallic nanoparticles.

## Sensing atrazine with cyclic voltammetry

Complementary, Fig. 7 shows voltammograms obtained to check the sensing performance of the cyclic voltammetry technique in terms of atrazine detection using the same kind of thin films applied to impedance spectroscopy, i. e., PAH/AuNPs and PAH/AgNPs LbL films, however, now to modify the ITO electrodes (instead of Pt interdigitated electrodes). The cyclic voltammograms obtained for both modified electrodes show one anodic peak at −571 mV versus Ag/AgCl, which may be associated with $InO_3$ at

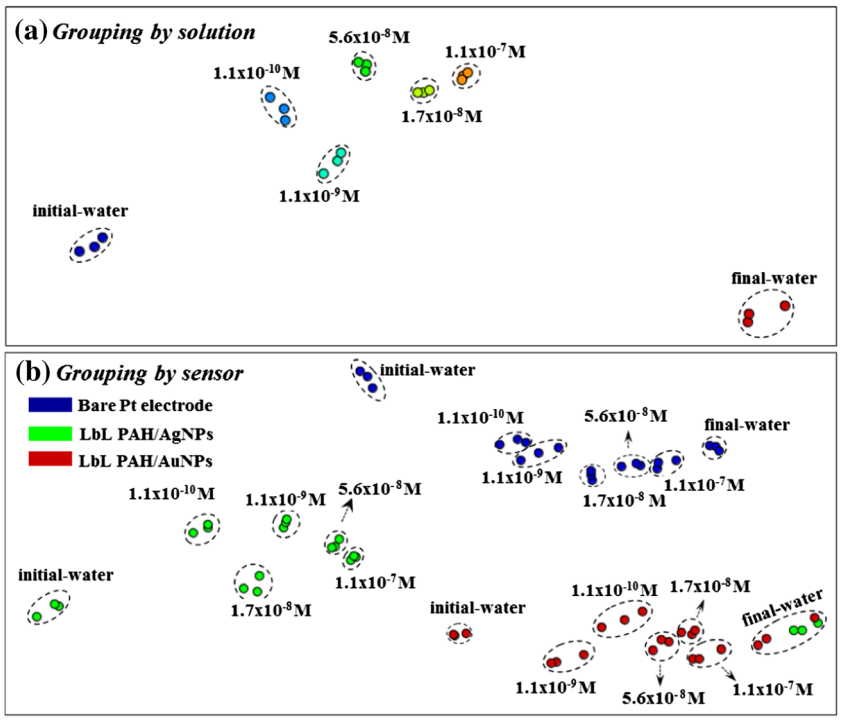


**Fig. 6** IDMAP projection of the capacitance data obtained **a** from all sensing units combined in a single projection to discriminate the solution concentrations. **b** Data of all sensing units separately projected on a single graph

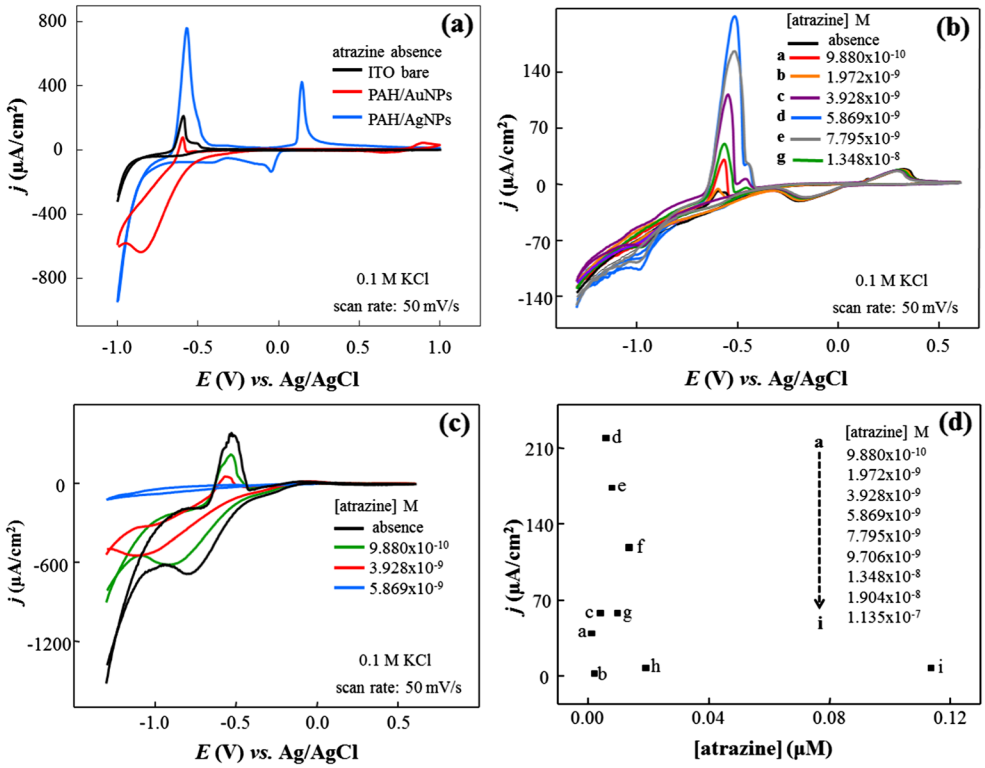


**Fig. 7** **a** Cyclic voltammograms of ITO bare electrode, ten bilayers of PAH/AgNPs and ten bilayers of PAH/AuNPs-modified electrodes in the absence of atrazine in solution. Cyclic voltammograms for **b** PAH/AgNPs and **c** PAH/AuNPs in the presence of different atrazine concentrations. All measurements were carried out at 0.1-M KCl solution as supporting electrolyte at pH 1.88 and with 50 mV $s^{-1}$. **d** Variation of absolute current values of PAH/AgNP-modified electrode versus atrazine concentration

low pH values ($InO_3$ present on ITO electrode surface). The PAH/AgNPs-modified electrode presented a redox process at $E_{pa}$=148 mV and $E_{pc}$=−42 mV versus Ag/AgCl, which is ascribed to the oxidation of Ag and the reduction of Ag oxides on the ITO electrode surface [51], while the PAH/AuNPs-modified electrode presented a redox process at $E_{pa}$=895 mV and $E_{pc}$=654 mV versus Ag/AgCl, which is ascribed to reduction of Au oxides at the nanoparticles [52]. In the presence of atrazine in solution, the PAH/AgNPs-modified electrode showed a nonlinear variation of the current values with an increase of atrazine concentration. Thus, it was not possible to obtain the analytical curve. Anyway, the lowest concentration that we were able to measure was limited at $10^{-9}$ M. On the other hand, a great decrease of current values in the presence of atrazine was observed for PAH/AuNPs-modified electrodes, which may be related to loss of charge transfer. Indeed, the AgNPs showed to be more sensitive to the presence of atrazine in solution, however, without a linear variation with atrazine concentration, while AuNP response was not favorable to atrazine determination. The latter results reinforced the potential of SERS as a suitable tool to detect atrazine above and below its concentration limit allowed for drinking water.

## Conclusions

We have shown that SERS can be used to detect atrazine in AgNPs colloid with the lowest concentration ever reported to the best of our knowledge, where distinction was made absolutely clear using a Sammon's mapping plot. Most significantly, distinguishing an atrazine concentration down to $5\times10^{-12}$ M, as was done here, is sufficient to monitor the quality of drinking water even according to the most stringent international regulations and is an important step toward single-molecule detection. The importance of detection via SERS was further illustrated in a comparative study where atrazine was detected in aqueous solutions using the e-tongue concept with impedance spectroscopy and cyclic voltammetry applied to LbL films made with AuNPs and AgNPs. Though distinction of the different concentrations of atrazine could be made using impedance spectroscopy, we noted that the electrodes were irreversibly affected by the measurements, a limitation that does not apply to SERS. Finally, the analysis of SERS data with information visualization methods, which only recently has been introduced [43] and was exploited here, paves the way for detecting atrazine and other pesticides in real samples of drinking water.

**Acknowledgments** This work was supported by the Brazilian agencies FAPESP, CNPq and CAPES and by the nBioNet network.

## References


1. Belden JB, Hanson BR, McMurry ST, Smith LM, Haukos DA (2012) Assessment of the effects of farming and conservation programs on pesticide deposition in high plains wetlands. Environ Sci Technol 46(6):3424–3432. doi:10.1021/es300316q
2. Knauert S, Escher B, Singer H, Hollender J, Knauer K (2008) Mixture toxicity of three photosystem II inhibitors (atrazine, isoproturon, and diuron) toward photosynthesis of freshwater phytoplankton studied in outdoor mesocosms. Environ Sci Technol 42(17): 6424–6430. doi:10.1021/es072037q
3. Prade L, Huber R, Bieseler B (1998) Structures of herbicides in complex with their detoxifying enzyme glutathione S-transferase - explanations for the selectivity of the enzyme in plants. Struct Fold Des 6(11):1445–1452. doi:10.1016/s0969-2126(98)00143-9
4. Kucka M, Pogrmic-Majkic K, Fa S, Stojilkovic SS, Kovacevic R (2012) Atrazine acts as an endocrine disrupter by inhibiting cAMP-specific phosphodiesterase-4. Toxicol Appl Pharmacol 265(1):19–26. doi:10.1016/j.taap.2012.09.019
5. Rusiecki JA, De Roos A, Lee WJ, Dosemeci M, Lubin JH, Hoppin JA, Blair A, Alavanja MCR (2004) Cancer incidence among pesticide applicators exposed to atrazine in the agricultural health study. J Natl Cancer Inst 96(18):1375–1382
6. Simpkins JW, Swenberg JA, Weiss N, Brusick D, Eldridge C, Stevens JT, Handa RJ, Hovey RC, Plant TM, Pastoor TP, Breckenridge CB (2011) Atrazine and breast cancer: a framework assessment of the toxicological and epidemiological evidence. Toxicol Sci 123(2):441–459. doi:10.1093/toxsci/kfr176
7. Kuklenyik Z, Panuwet P, Jayatilaka NK, Pirkle JL, Calafat AM (2012) Two-dimensional high performance liquid chromatography separation and tandem mass spectrometry detection of atrazine and its metabolic and hydrolysis products in urine. J Chromatogr B Anal Technol Biomed Life Sci 901:1–8. doi:10.1016/j.jchromb.2012.05.028
8. Bono L, Magi E (2013) Fast and selective determination of pesticides in water by automated on-line solid phase extraction liquid chromatography tandem mass spectrometry. Anal Lett 46(10):1467–1476. doi:10.1080/00032719.2013.769263
9. dos Santos LBO, Silva MSP, Masini JC (2005) Developing a sequential injection-square wave voltammetry (SI-SWV) method for determination of atrazine using a hanging mercury drop electrode. Anal Chim Acta 528(1):21–27. doi:10.1016/j.aca.2004.10.008
10. Guse D, Bruzek MJ, DeVos P, Brown JH (2009) Electrochemical reduction of atrazine: NMR evidence for reduction of the triazine ring. J Electroanal Chem 626(1–2):171–173. doi:10.1016/j.jelechem.2008.12.006
11. Dai C, Feng B, Cheng Y, Ding Y, Fei J (2013) Direct electrochemistry of cytochrome p450 enzyme in polyethylene glycol-acetylene black composite film and its application for the determination of atrazine. Nanosci Nanotechnol Lett 5(6):677–683. doi:10.1166/nnl.2013.1587
12. Pardieu E, Cheap H, Vedrine C, Lazerges M, Lattach Y, Garnier F, Ramita S, Pernelle C (2009) Molecularly imprinted conducting polymer based electrochemical sensor for detection of atrazine. Anal Chim Acta 649(2):236–245. doi:10.1016/j.aca.2009.07.029
13. Piletsky SA, Piletskaya EV, Elgersma AV, Yano K, Karube I, Parhometz YP, Elskaya AV (1995) Atrazine sensing by moleculary imprinted membranes. Biosens Bioelectron 10(9–10):959–964. doi:10.1016/0956-5663(95)99233-b
14. Svorc L, Rievaj M, Bustin D (2013) Green electrochemical sensor for environmental monitoring of pesticides: determination of atrazine in river waters using a boron-doped diamond electrode. Sensors Actuator B Chem 181:294–300. doi:10.1016/j.snb.2013.02.036
15. http://water.epa.gov/drink/contaminants/basicinformation/atrazine.cfm#four. Accessed 04/08/2013
16. http://ec.europa.eu/food/plant/protection/evaluation/existactive/list_atrazine.pdf. Accessed 04/08/2013 2013
17. Fleischmann M, Hendra PJ, McQuillan AJ (1974) Raman-spectra of pyridine adsorbed at a silver electrode. Chem Phys Lett 26(2):163–166. doi:10.1016/0009-2614(74)85388-1
18. Aroca R (2006) Surface-enhanced vibrational spectroscopy. John Wiley & Sons, Chichester
19. Le Ru EC, Etchegoin PG (2009) Principles of surface enhanced Raman spectroscopy (and related plasmonic effects). Elsevier, Amsterdam
20. Aoki PHB, Furini LN, Alessio P, Aliaga AE, Constantino CJL (2013) Surface-enhanced Raman scattering (SERS) applied to cancer diagnosis and detection of pesticides, explosives, and drugs. Rev Anal Chem 32(1):55–76. doi:10.1515/revac-2012-0019
21. Cabrer FC, Aoki PHB, Aroca RF, Constantino CJL, dos Santos DS, Job AE (2012) Portable smart films for ultrasensitive detection and chemical analysis using SERS and SERRS. J Raman Spectrosc 43(4):474–477. doi:10.1002/jrs.3074
22. Kneipp K, Wang Y, Kneipp H, Perelman LT, Itzkan I, Dasari R, Feld MS (1997) Single molecule detection using surface-enhanced Raman scattering (SERS). Phys Rev Lett 78(9):1667–1670. doi:10.1103/PhysRevLett.78.1667
23. Nie SM, Emery SR (1997) Probing single molecules and single nanoparticles by surface-enhanced Raman scattering. Science 275(5303):1102–1106. doi:10.1126/science.275.5303.1102
24. Constantino CJL, Lemma T, Antunes PA, Aroca R (2001) Single-molecule detection using surface-enhanced resonance Raman scattering and Langmuir-Blodgett monolayers. Anal Chem 73(15):3674–3678. doi:10.1021/ac0101961
25. Xie Y, Mukamurezi G, Sun Y, Wang H, Qian H, Yao W (2012) Establishment of rapid detection method of methamidophos in vegetables by surface enhanced Raman spectroscopy. Eur Food Res Technol 234(6):1091–1098. doi:10.1007/s00217-012-1724-9
26. Yazdi SH, White IM (2013) Multiplexed detection of aquaculture fungicides using a pump-free optofluidic SERS microsystem. Analyst 138(1):100–103. doi:10.1039/c2an36232e
27. Zhang L (2013) Self-assembly Ag nanoparticle monolayer film as SERS Substrate for pesticide detection. Appl Surf Sci 270:292–294. doi:10.1016/j.apsusc.2013.01.014
28. Liu B, Zhou P, Liu X, Sun X, Li H, Lin M (2013) Detection of pesticides in fruits by surface-enhanced Raman spectroscopy coupled with gold nanostructures. Food Bioproc Technol 6(3):710–718. doi:10.1007/s11947-011-0774-5
29. Riul A, dos Santos DS, Wohnrath K, Di Tommazo R, Carvalho A, Fonseca FJ, Oliveira ON Jr, Taylor DM, Mattoso LHC (2002) Artificial taste sensor: efficient combination of sensors made from Langmuir-Blodgett films of conducting polymers and a ruthenium complex and self-assembled films of an azobenzene-containing polymer. Langmuir 18(1):239–245. doi:10.1021/la011017d
30. Aoki PHB, Volpati D, Cabrera FC, Trombini VL, Riul A Jr, Constantino CJL (2012) Spray layer-by-layer films based on phospholipid vesicles aiming sensing application via e-tongue system. Mater Sci Eng C Mater Biol Appl 32(4):862–871. doi:10.1016/j.msec.2012.02.004
31. Crespilho FN, Zucolotto V, Siqueira JR, Constantino CJL, Nart FC, Oliveira ON Jr (2005) Immobilization of humic acid in nanostructured layer-by-layer films for sensing applications. Environ Sci Technol 39(14):5385–5389. doi:10.1021/es050552n
32. Lee PC, Meisel D (1982) Adsorption and surface-enhanced Raman of dyes on silver and gold sols. J Phys Chem 86(17):3391–3395. doi:10.1021/j100214a025

33. Leopold N, Lendl B (2003) A new method for fast preparation of highly surface-enhanced Raman scattering (SERS) active silver colloids at room temperature by reduction of silver nitrate with hydroxylamine hydrochloride. J Phys Chem B 107(24):5723–5727. doi:10.1021/jp027460u
34. Aoki PHB, Alessio P, Antonio De Saja J, Leopoldo Constantino CJL (2010) Incorporation of Ag nanoparticles into membrane mimetic systems composed by phospholipid layer-by-layer (LbL) films to achieve surface-enhanced Raman scattering as a tool in drug interaction studies. J Raman Spectrosc 41(1):40–48. doi:10.1002/jrs.2415
35. Gorban A, Kegl B, Wunsch D, Zinovyev A (2007) Principal manifolds for data visualisation and dimension reduction. Springer, Berlin
36. Oliveira ON, Jr., Pavinatto FJ, Constantino CJL, Paulovich FV, de Oliveira MCF (2012) Information visualization to enhance sensitivity and selectivity in biosensing. Biointerphases 7 (1-4). doi:53 10.1007/s13758-012-0053-7
37. Tejada E, Minghim R, Nonato LG (2003) On improved projection techniques to support visual exploration of multi-dimensional data sets. Inf Vis 2:218–231
38. Sammon JW Jr (1969) A nonlinear mapping for data structure analysis. IEEE Trans Comp C-18(5):401–409. doi:10.1109/t-c.1969.222678
39. Minghim R, Paulovich FV, Lopes ADA (2006) Content-based text mapping using multi-dimensional projections for exploration of document collections. In: Erbacher RF, Roberts JC, Grohn MT, Borner K (eds) Visualization and data analysis 2006, vol 6060. Proceedings of SPIE. doi:60600 s 10.1117/12.650880
40. Costa JCS, Ando RA, Camargo PHC, Corio P (2011) Understanding the effect of adsorption geometry over substrate selectivity in the surface-enhanced Raman scattering spectra of simazine and atrazine. J Phys Chem C 115(10):4184–4190. doi:10.1021/jp112021j
41. Bonora S, Benassi E, Maris A, Tugnoli V, Ottani S, Di Foggia M (2013) Raman and SERS study on atrazine, prometryn and simetryn triazine herbicides. J Mol Struct 1040:139–148. doi:10.1016/j.molstruc.2013.02.025
42. Paulovich FV, Moraes ML, Maki RM, Ferreira M, Oliveira ON Jr, de Oliveira MCF (2011) Information visualization techniques for sensing and biosensing. Analyst 136(7):1344–1350. doi:10.1039/c0an00822b
43. Aoki PHB, Carreon EGE, Volpati D, Shimabukuro MH, Constantino CJL, Aroca RF, Oliveira ON Jr, Paulovich FV (2013) SERS mapping in Langmuir-Blodgett films and single-molecule detection. Appl Spectrosc 67(5):563–569. doi:10.1366/12-06909
44. Tolaieb B, Constantino CJL, Aroca RF (2004) Surface-enhanced resonance Raman scattering as an analytical tool for single molecule detection. Analyst 129(4):337–341. doi:10.1039/b312812a
45. Aoki PHB, Alessio P, Riul A Jr, De Saja Saez JA, Constantino CJL (2010) Coupling surface-enhanced resonance Raman scattering and electronic tongue as characterization tools to investigate biological membrane mimetic systems. Anal Chem 82(9):3537–3546. doi:10.1021/ac902585a
46. Carrillo-Carrion C, Simonet BM, Valcarcel M, Lendl B (2012) Determination of pesticides by capillary chromatography and SERS detection using a novel Silver-Quantum dots "sponge" nanocomposite. J Chromatogr A 1225:55–61. doi:10.1016/j.chroma.2011.12.002
47. Riul A Jr, Dantas CAR, Miyazaki CM, Oliveira ON Jr (2010) Recent advances in electronic tongues. Analyst 135(10):2481–2495. doi:10.1039/c0an00292e
48. Taylor DM, Macdonald AG (1987) AC admittance of the metal-insulator-electrolyte interface. J Phys D Appl Phys 20(10):1277–1283. doi:10.1088/0022-3727/20/10/010
49. Riul A, Soto AMG, Mello SV, Bone S, Taylor DM, Mattoso LHC (2003) An electronic tongue using polypyrrole and polyaniline. Synth Met 132(2):109–116. doi:10.1016/s0379-6779(02)00107-8
50. Zaretsky MC, Mouayad L, Melcher JR (1988) Continuum properties from interdigital electrode dielectrometry. IEEE Trans Electr Insul 23(6):897–917. doi:10.1109/14.16515
51. Chang G, Zhang JD, Oyama M, Hirao K (2005) Silver-nanoparticle-attached indium tin oxide surfaces fabricated by a seed-mediated growth approach. J Phys Chem B 109(3):1204–1209. doi:10.1021/jp046652h
52. Crespilho FN, Zucolotto V, Brett CMA, Oliveira ON Jr, Nart FC (2006) Enhanced charge transport and incorporation of redox mediators in layer-by-layer films containing PAMAM-encapsulated gold nanoparticles. J Phys Chem B 110(35):17478–17483. doi:10.1021/jp062098v